Segmented Mirror Coarse Phasing with White Light Interferometry: Modeling and Experiment on NGST's Wavefront Control Testbed

Fang Shi[a], David C. Redding[a], Andrew E. Lowman[a], Catherine M. Ohara[a], Laura A. Burns[b], Peter Petrone III[b], Charles W. Bowers[b], and Scott A. Basinger[a]

[a]Jet Propulsion Laboratory, California Institute of Technology, Pasadena, CA 91109
[b]Goddard Space Flight Center, NASA, Greenbelt, MD 20771

ABSTRACT

A method of coarse phasing segmented mirrors using white light interferometry (WLI) has been developed for Next Generation Space Telescope (NGST) wavefront sensing and control. Using the broadband point spread function (PSF) of the segmented mirrors taken during a segment piston scan, the WLI can accurately detect small residual piston errors. WLI does not rely on any extra optics and uses only the final imaging camera. With its high sensitivity to small segment piston error WLI can be used as a complementary phasing algorithm to the dispersed fringe sensor (DFS) for NGST. The paper will present the results from modeling and experiment on the NGST's Wavefront Control Testbed (WCT).

Keywords: Space telescope, segmented mirror, wavefront sensing and control, white light interferometry

1. INTRODUCTION

Segmented mirror coarse phasing is part of the Next Generation Space Telescope (NGST) wavefront sensing and control (WFS&C) process during the early stage of NGST commissioning [1]. It begins after coarse alignment, the process which includes initial capture, tip-tilt alignment, and focusing of each segmented mirror. After coarse alignment the segmented mirrors are aligned with the residual tilt errors no larger than a fraction of the point spread function (PSF), and focused within a depth-of-focus (DOF) of each segmented mirror. Although the residual tilts can be handled by the fine phasing, the residual relative pistons (with amplitudes of ~1 DOF) are still many orders of magnitude too large to be phased by the fine phasing algorithm [2]. Coarse phasing with a dispersed fringe sensor (DFS) has been proposed as the segmented mirror coarse phasing technique for NGST baseline wavefront sensing and control [3, 4] and it has shown to have adequate dynamic range and accuracy for NGST. However, we have proposed and studied another coarse phasing technique based on the white light interferometry (WLI). Segmented mirror coarse phasing with WLI uses the features of the white light point spread function (PSF) formed by the segmented mirrors to detect and correct the relative piston between segments. Compared with DFS, the coarse phasing with WLI uses only in-focus PSF and requires no special optics (grism), and with accurate piston actuators the WLI can provide piston detection sensitivity better than a few tens of nanometers. However, coarse phasing with WLI needs to take a large number of in-focus images of a point source as the segment being pistoned. This practically limits the WLI's piston detection range to a few microns around the phased position. With its limited range but higher accuracy than DFS, the WLI can be used as next step of coarse phasing after the DFS. There exists other technique that utilizes the features of a broadband PSF to phase the segment mirrors and some are currently being used for the ground based telescope [5]. The method we proposed, however, gives direct measurement of the segment pistons and requires no special optics. This is significantly beneficial for space telescope such as NGST.

The WLI piston detection algorithm was developed using the realistic optical models. Optical models of various segmented mirror configurations have been establish and used to generate white light PSF. The WLI algorithm has been tested on NGST's Wavefront Control Testbed (WCT). With three segmented mirrors and two deformable mirrors the WCT provides a flexible testing environment. Various tests have been designed to explore the performance of WLI and influence factors that may affect the WLI performance. The WLI tests on WCT have not only validated the algorithm

but also produced the WLI coarse phasing software as a part of the WCT's Segmented Telescope Control Software (STCS) which enables user to routinely phasing the segmented mirror on the WCT [6].

In this paper we will introduce the principle of the segmented mirror coarse phasing with white light interferometry. We will use the results from both the model simulations and NGST's Wavefront Control Testbed (WCT) experiment to show how the coarse phasing with WLI works. We will discuss the performance and the characteristics of WLI from the point of view of NGST operation, and finally we will layout the plans for the future studies of WLI.

2. WHITE LIGHT INTERFEROMETRY FOR SEGMENTED MIRROR PISTON DETECTION

The wavefront of a telescopes with the segmented mirrors is combined from the wavefront of each individual segments and the broadband PSF from the segmented mirrors can be seen as the result of the white light interferences of the segments. At the image plan, the phases of the electromagnetic field from two segments which have a relative wavefront piston δL is

$$\begin{aligned} \phi_1 &\sim e^{ikL} \cdot e^{-i\omega t}, \\ \phi_2 &\sim e^{ik(L+\delta L)} \cdot e^{-i\omega t} \end{aligned} \tag{1}$$

where $k = 2\pi/\lambda$ is the wave number L is the common path length. The time averaged the intensity at the image plane can be written as

$$I(\theta) = 2I_{seg}(\theta) \cdot \left[1 + \gamma \cos\left(\frac{2\pi}{\lambda} (d\theta + \delta L) \right) \right] \tag{2}$$

where θ is the angular image plane coordinate, d is the base line distance between the two segments, and $I_{seg}(\theta)$ is the PSF of one segment mirror. The visibility constant γ is determined by factors such as the source size, the segment mirror figure error, or if there present other segments to contribute to the total intensity of $I(\theta)$. For the case of two ideal segments with equal area illuminated by a point source the visibility $\gamma = 1$. For a circular segmented mirror with diameter of D the single segment PSF $I_{seg}(\theta)$ is simply

$$I_{seg}(\theta) = A \cdot \left[\frac{2J_1(\pi\theta D/\lambda)}{\pi\theta D/\lambda} \right]^2 D^2 \tag{3}$$

Eq. 2 shows that the relative wavefront piston between the segmented mirrors will form an intensity modulation within the envelope of the PSF formed by the segments $I_{seg}(\theta)$. The Intensity modulation depends on the wavefront piston as well as the wavelength, forming a dark band I_{max} and bright band I_{min} when conditions are as follows:

$$\begin{aligned} I_{\min} &\Leftrightarrow \frac{2\pi}{\lambda}(d\theta + \delta L) = (2n-1)\pi \\ I_{\max} &\Leftrightarrow \frac{2\pi}{\lambda}(d\theta + \delta L) = 2n\pi \end{aligned} \tag{4}$$

while $n = 1, 2, \ldots$is an integer. Therefore, for monochromatic light as the piston δL increases the modulation within the PSF will repeat. If we try to use the modulation relations defined in Eq. 4 to detect the segment relative piston δL we would encounter the ambiguity problem which we can not determine the integer n in Eq. 4. However, the ambiguity problem can be solved by using the white light – a source with wide spectral bandwidth. When integrate the Eq. 3 over the white light source with wavelength bandwidth of $\Delta\lambda$ centered at λ_0 the center ($\theta = 0$) intensity $I(0)$ will have the form of [7],

$$I = 2I_{seg}(0)\cdot\Delta\lambda\left[1+\gamma\left(\frac{\sin\left(\frac{\pi\Delta\lambda}{\lambda_0^{\,2}}\delta L\right)}{\frac{\pi\Delta\lambda}{\lambda_0^{\,2}}\delta L}\right)\cos\left(\frac{2\pi}{\lambda}\delta L\right)\right] \tag{5}$$

The sinc function Eq 5 shows that for a broadband source the visibility of the modulation due to the piston will depend on the spectral bandwidth $\Delta\lambda$ as well as the piston error δL. In addition, the intensity modulations within the PSF is most visible when the piston error δL is smaller than the coherence length defined as $\lambda_0^2/\Delta\lambda$. Segmented mirror coarse phasing with white light interferometry (WLI) uses this intensity modulation within the broadband PSF to sense the relative piston between the segments.

Figure 1 is a modeled WCT WLI signal which uses the center pixel intensity versus segment piston position. While one segment is piston scanned from δL = –5 μm to +5 μm with step size of 0.01 μm a broadband PSF image is generated for each piston position. The WLI signal is formed from the center pixel intensity of the image. The under-sampled image in WCT has lowered the visibility but as shown in the figure the modulation is still quite strong. Two broad wavelength bandwidths are simulated here to reflect the testbed source setup, one with FWHM bandwidth of 220 nm and another 300 nm. Figure 2 shows some sampled PSF images of the piston scan around segments being phased. For the purpose of comparison the piston values selected are the same for both filter bandwidth. Compare to plots in Figure 1 we can see the effect of wavelength bandwidth and coherent length on the WLI signal: broader bandwidth narrows the piston range of which the PSF modulation is visible.

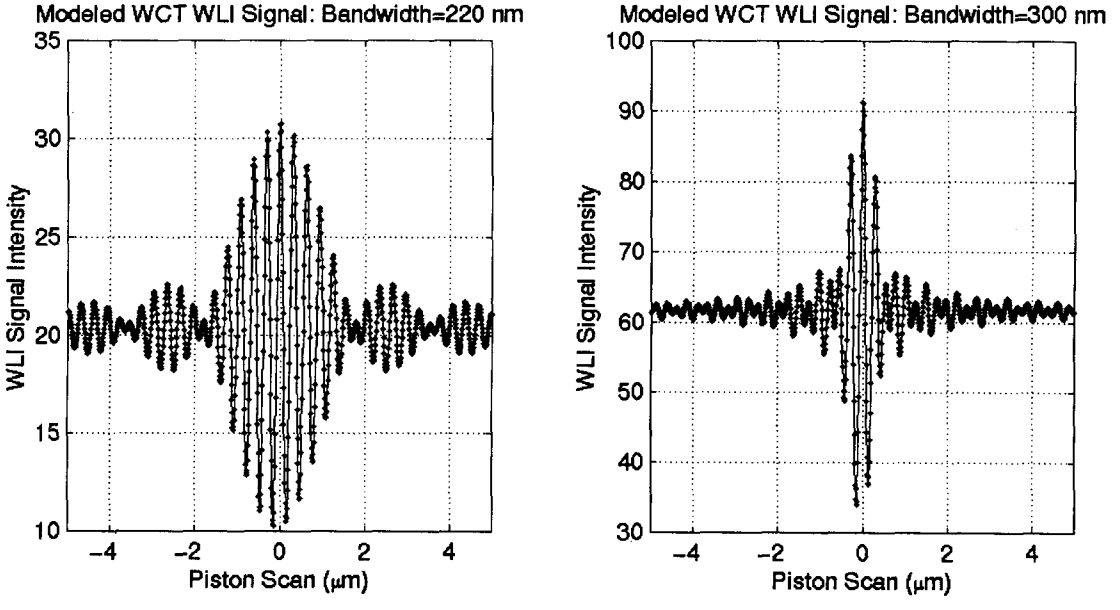

Figure 1. Modeled WCT broadband PSF center pixel intensity versus segment #3 piston position. Segment #1 is used as the reference segment. *Left*: WLI signal with 220 nm bandwidth; *Right*: WLI signal with 300 nm bandwidth. Both wavelength filters are centered at 633 nm and the model assumes a flat spectrum.

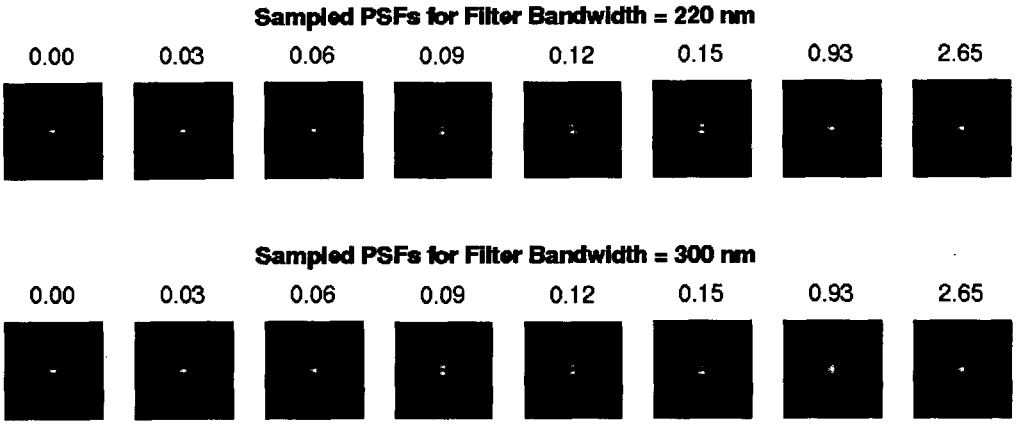

Figure 2. Selected sample PSF images from the WLI piston scan. The piston values are shown on top of each image in unit of micron. *Top row*: WLI PSFs with 220 nm bandwidth; *Bottom row*: WLI PSFs with 300 nm bandwidth.

The process of using WLI to sense and remove the relative segment piston is as follows: First, the segmented system needs a broadband point source. As indicated in the Eq. 2 a resolvable source will lower the visibility of the modulation. Second, select correspondent wavelength filter bandwidth and piston scan range according to the estimated segment piston. The coherent length should be larger than the piston to be detected. When the segments are phased with a DFS, which can reduce the piston error to within 0.1 μm, a broader bandwidth filter (> *300 nm*) can be used for taking WLI signal. The piston scanning range which centered at current segment position is determined according to the selected filter, narrower the wavelength filter larger the piston scan range. Third, scans the piston of the segment to be phased with a small step size. Take image at each piston step and record segment piston position. The minimal piston scanning step size, which related to the WLI piston sensitivity, is determined by the segment aperture size and base line distance between the two segments. Forth, extract the center pixel intensity from each piston scanning PSF image. For the data from WCT, which currently does not have a closed loop faster mirror, centroid calculation is required to determine the center pixel. The relation of this PSF center pixel intensity versus piston position is the WLI signal for that segment. Finally, from the WLI signal the piston position at which WLI signal is at maximum is the piston of the segment. However, due the detector noise and environmental variations during the process of taking the WLI signal, detecting the piston directly using peak intensity of WLI is not reliable. Instead, we use the cross correlation between the measured WLI signal and the ideal WLI template generated from modeling to find the piston position at which the WLI is at maximum. The cross correlation uses all the points in the WLI signal which significantly reduces the influence of the noise fluctuation in the signal, resulting a more reliable piston detection. The Figure 3 shows the results from a WCT simulation with one segmented had a piston error of –1.0 μm. To demonstrate the effectiveness of detecting segment piston with correlation random noises which equal to 10% of full peak intensity of PSFs were added to the WLI signals, resulting a very noisy WLI signal. However, because correlation method uses all the points of WI signal the correlated signal is very clean, which in turn provides more robust and accurate piston detection. For the WLI signal shown in Figure 3 using the peak intensity of WLI signal to detect the piston would detect a piston of –1.04 μm while using the correlation the result would be –1.00 μm.

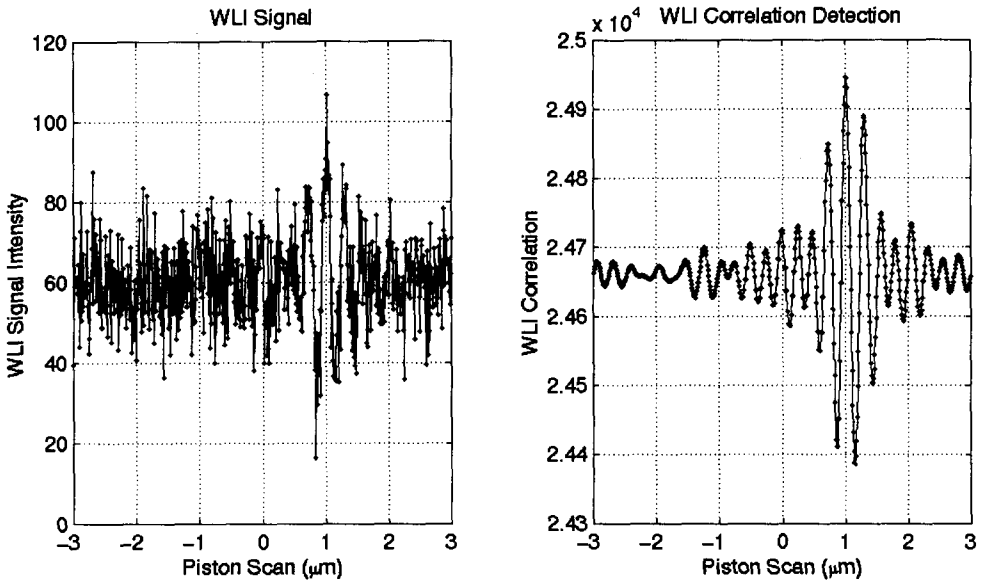

Figure 3. *Right*: Modeled WCT WLI signal with segment #3 is pistoned down by –1.0 μm while segment #2 is used as the reference segment. Significant amount of random noises were added to the WLI piston scan images, resulting a very noisy WLI signal. *Left*: The cross correlation with the ideal template to detect the segment piston.

Once the segment piston is measured by WLI the control software can drive the segment to remove the segment piston and therefore phase the two segments. The phased segments are then used as the reference segment and the process repeats again to phase the remaining segments until all the segments are phased. As more segments built up as the reference the aperture area difference between the reference segment and the segment being phased will increase. This will reduce the modulation within the PSF (γ in Eq. 2) and therefore reduce the visibility of WLI signal. For a segmented system which have a large number of segmented mirrors the segments can be grouped and PSF centers of these groups be separated so that each piston scanning image will contain a PSF for each group. In this fashion the WLI process can be done separately and in parallel for each group. After having phased all the segments within each group then each phased group can be treated as one segment and the WLI will phase the "group segments" together to form an all phased aperture. The segment grouping will not only increase the WLI efficiency but also avoid the poor WLI signal visibility due to segments building up.

3. WLI EXPERIMENTS ON WAVEFRONT CONTROL TESTBED

The NGST's WCT is modular system which consists of (1) the Source Module which can provide both narrow and broad band point sources; (2) the Simulator Module which can generate high order aberrations using a 69-actuator deformable mirror (SMDM) and a wavefront piston using a set of transmissive phase plates, or contains three segmented mirrors that each can be accurately tilted and pistoned; (3) the Aft-Optics Module which contains a one-to-one imaging system, a 349-actuator deformable mirror (AODM) for wavefront correction, a fast steering mirror, a flip-in grism, and a CCD camera on a translation stage. The segmented mirrors in the WCT consist of three one-inch diameter spherical mirrors. The segmented mirrors are conjugated to the testbed system aperture which is defined by the Aft-Optical DM. Each segmented mirror is driven by a PZT platform with 3 piezoelectric actuators which provide 12 μm accurate actuations. Compare to the full aperture of DM the three segmented mirror form a sparse aperture with the segmented mirrors cover only about 30% of total aperture area formed by DM. The WCT is physically located at Goddard Space Flight Center and most of the experiments are run via the Internet from JPL by the WCT's Segmented Telescope Control Software (STCS) [6]. More detailed information of about the WCT hardware setup and capability can be found in references [8, 9].

In the WLI experiment the user graphic interface (GUI) designed for WCT's WLI allows user to select the reference segment(s), the segment to be phased, the wavelength filter, and to specify the WLI piston scanning range and step size. To limit the number of images needed, WLI experiment on WCT is usually started after the processes of WCT coarse alignment and coarse phasing with a DFS. Due to the testbed environment perturbations such as the lab seeing, testbed jittering, and testbed drifting the PSF images taking during the piston scan are blurred and the PSF centroid positions are moved around by as much as a pixel. To extract the WLI signals from the center pixel of the PSFs the centroid of the PSF is calculated and WLI signal is interpolated at the center position of each PSF. The fact that the WCT's PSF is under sampled has worsen the situation and caused more fluctuation of the WLI signal. As mentioned in Section 2 using the whole WLI signal to cross correlate with the template reduces the influence of the WLI signal fluctuation. Figure 4 demonstrates the close loop performance of WLI on the WCT. The plots show the broadband PSFs and WLI signals before and after the piston correction. The final residual piston is related to the piston scan step size and the WLI shows that there is 20 nm residual piston which is equal the piston step size in the experiment. An independent wavefront sensing using the in-focus PSF optimizer (IPO) [10] was performed after the WLI correction and has verified that the residual piston on the segment was 13 nm.

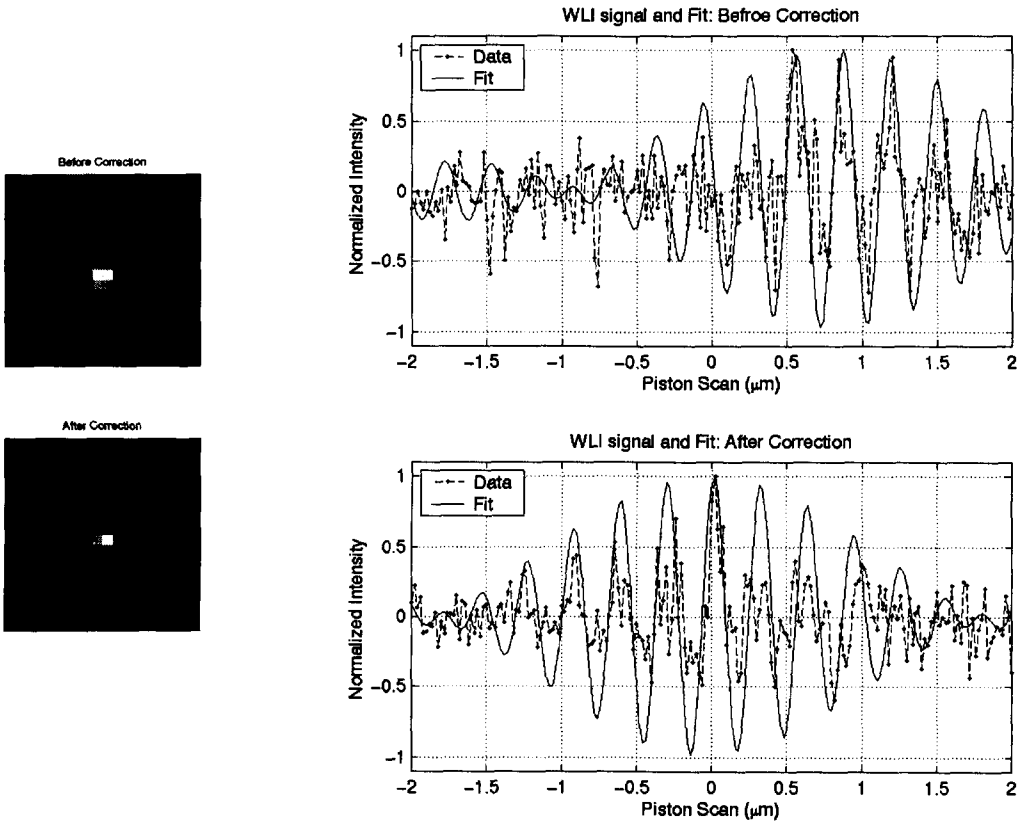

Figure 4. WLI close loop demonstration on WCT: segment #2 is the reference and segment #3 is being phased. *Upper left*: broadband PSF before segments being phased. *Upper right*: WLI signal and WLI piston solution fit before the correction. The WLI has detected the segment #3 piston is –0.88 μm. *Lower left*: broadband PSF after being phased. *Lower right*: WLI signal and WLI piston solution fit after the correction. The WLI has detected a residual piston of 20 nm. The 220 nm filter is used for this experiment.

Tests were also done to study the effect of segment building up on WCT. In the experiment, first a WLI signal was taken with only one reference segment in. Then a WLI signal was taken with two phased segments as the reference segment. The WLI signals as well as PSFs at which the WLI signals are at maximal are shown in Figure 5. The WLI signals and the PSFs have shown that there are two opposite effects of the segment building up: on one hand, as more segments are

included in as the reference segments the mean WLI signal level increases because the total collecting aperture area increases. This will lower the WLI signal visibility and increase the photon noise hence lower the signal to noise ratio (SNR) of WLI. On the other hand, however, as more segments being phased the peak intensity oscillation of WLI signal will increase because the PSF size is smaller due to the total area increase. This will increase the WLI signal's SNR. The end result of the segment building up depends on the image sampling, aperture sparseness, and segment base line distance. Simulation has shown that for a system with large number of segments the adverse effect of segments building up is dominant and phasing segment by grouping the segment is a more suitable approach.

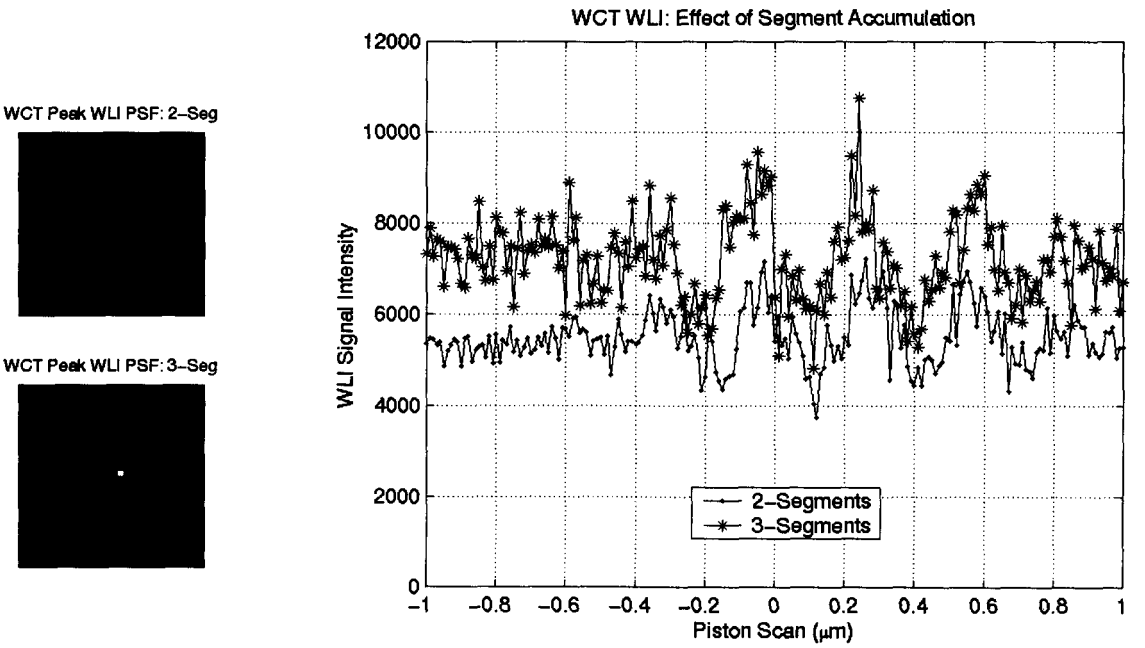

Figure 5. WCT WLI Experiment on the effect of segments building up. *Left panel*: PSFs when WLI signal intensity is at maximal. The top image is from 2 segments and the bottom is that of 3 segments. *Right panel*: Comparison of WLI signals with one and two segments reference. The WLI signal from the 3 segments is higher due to the larger collecting area.

4. CONCLUSIONS AND FUTURE WORKS

Segmented mirror coarse phasing with white light interferometry is a different approach of the coarse phasing compared with the dispersed fringe sensor. WLI provides finer piston sensitivity (*10 ~ 20 nm*) but required more images than DFS. Because the WLI uses the piston scan as the its signal the WLI segment piston sensing and correcting also depends on the linearity and accuracy of the segmented mirror actuators. In the NGST wavefront sensing and control, the process of coarse phasing with a DFS has already provided enough dynamic range and accuracy to handle the segment piston between the coarse alignment and fine phasing [4]. However, since it requires no other special optics other than a broadband filter the WLI can be used as an alternate segment piston sensing and control method for NGST.

Experiment on WCT has validated the modeling results and demonstrated the closed loop performance of WLI on the testbed. Coarse phasing with WLI algorithm has been used in the routine operation of the testbed and the WLI control software has been integrated with testbed's STCS.

More modeling studies and WCT WLI experiments will follow. These include tests to explore the WLI robustness against the adverse influence such as the segmented mirror surface aberrations and radius mismatch. Modeling and experiment will also be carried out to define the best strategy of choosing wavelength filter bandwidth and piston

scanning range and step size to optimize the WLI dynamic range and final accuracy. The WCT is evolving and will provide us with more test capability as well as close to the real NGST hardware characteristics.

5. ACKNOWLEDGEMENTS

The work reported here is the result of effort from all the members in the NGST wavefront sensing and control team both at Jet Propulsion Laboratory and Goddard Space Flight Center. This work was performed at the Jet Propulsion Laboratory, California Institute of Technology, under contract with the National Aeronautics and Space Administration.

6. REFERENCES

[1] D. Redding, S. Basinger, C. Bowers, R. Burg, L. Burns, D. Cohen, B. Dean, J. Green, A. Loman, C. Ohara, and F. Shi, "Next Generation Space Telescope wavefront sensing and control," SPIE paper 4850-49, Waikoloa, Hawaii (2002).

[2] D. Redding, S. Basinger, C. Bowers, L. Burns, D. Cohen, B. Dean, P. Dumont, J. Green, A. Loman, C. Ohara, and F. Shi, "Image-based wavefront sensing and control experiment," SPIE paper 4850-62, Waikoloa, Hawaii (2002).

[3] F. Shi, D. Redding, C. Bowers, A. Loman, S. Basinger, T. Norton, P. Petrone, P. Davila, M. Wilson, and R. Boucarut, "DCATT dispersed fringe sensor: modeling and experimenting with the transmissive phase plates," Proc. SPIE 4013, Munich, Germany (2000).

[4] F. Shi, D. Redding, A. Lowman, C. Bowers, L. Burns, P. Petrone, C. Ohara, and S. Basinger, "Segmented mirror coarse phasing with a dispersed fringe sensor: experiment on NGST's Wavefront Control Testbed," SPIE paper 4850-51, Waikoloa, Hawaii (2002).

[5] G. Chanan, J. Nelson, T. Mast, P. Wizinowich, and B. Schaefer, "The W. M. Keck Telescope Phasing Camera System," SPIE 2198, Kona, Hawai (1994).

[6] S. Basinger, D. Redding, F. Shi, D. Cohen, J. Green, C. Ohara, A. Lowman, L. Burns, "Wavefront sensing and control software for a segmented space telescope," SPIE paper 4850-56, Waikoloa, Hawaii (2002).

[7] "Principles of long baseline stellar interferometr," P. R. Lawson, editor, 1999.

[8] A. Lowman, F. Shi, D. Redding, S. Basinger, C. Bowers, and P. Davila, "Telescope simulator for the DCATT testbed," Proc. SPIE 4013, Munich, Germany (2000).

[9] P. Petrone, S. Basinger, C. Bowers, D. Cohen, L. Burns, A. Chu, P. Davila, P. Dogota, B. Dean, J. Green, K. Ha, W. Hayden, D. Lindler, A. Lowman, C. Ohara, D. Redding, F. Shi, M. Wilson, and B. Zukowski, "Optical design and performance of the NGST wavefront control testbed," SPIE paper 4850-55, Waikoloa, Hawaii (2002).

[10] C. Ohara, D. Redding, F. Shi, and J. Green, "PSF monitoring and in-focus wavefront control for NGST," SPIE paper 4850-64, Waikoloa, Hawaii (2002).